Dalton Transactions

An international journal of inorganic chemistry

Accepted Manuscript

This article can be cited before page numbers have been issued, to do this please use: J. K. Yadav, B. Singh, S. K. Pal, N. Singh, P. Lama, A. Indra and K. Kumar, *Dalton Trans.*, 2023, DOI: 10.1039/D2DT02511F.

ROYAL SOCIETY OF CHEMISTRY

rsc.li/dalton

Chlorocobaloxime Containing N-(4-pyridylmethyl)-1,8-naphthalamide Peripheral Ligands: Synthesis, Characterization and Enhanced Electrochemical Hydrogen Evolution in Alkaline Medium

Jitendra Kumar Yadav[a], Baghendra Singh[b], Sarvesh Kumar Pal,[a] Nanhai Singh,[a] Prem Lama[c*], Arindam Indra[b*], and Kamlesh Kumar[a*]

[a]Department of Chemistry, Institute of Science, Banaras Hindu University, Varanasi 221005, India.

[b]Department of Chemistry, Indian Institute of Technology (BHU), Varanasi, UP-221005, India.

[c]CSIR Indian Institute of Petroleum, Tech Block, Mohkampur, Dehradun 248005, Uttarakhand, India.

Abstract

Two new discrete cobaloxime based complexes with general formula [ClCo(dioxime)$_2$L] (**1** and **2**), $\mathbf{L_1}$ = N-(4-pyridylmethyl)-1,8-naphthalamide, $\mathbf{L_2}$ = 4-bromo-N-(4-pyridylmethyl)-1,8-naphthalamide have been synthesized and characterized by various spectroscopic techniques such as FT-IR, ^{1}H, ^{13}C{^{1}H} NMR and PXRD. Molecular structure of both complexes has also been determined using single crystal X-ray crystallography. The solid state molecular structures revealed distorted octahedral geometry around Co(III) central metal ion with two dioximes in the equatorial plan and axial positions are occupied by chloro and pyridine nitrogen of N-(4-pyridylmethyl)-1,8-naphthalamide ligands. Both complexes exhibit weaker non-covalent interactions such as C–H···O, C–H···Cl and C–H···π (Centroid) resulting in the formation of dimeric as well as 1D supramolecular structures. Further, these complexes are immobilized onto the surface of activated carbon cloth (CC) and their electrocatalytic performance for hydrogen evolution reaction (HER) have been investigated in the alkaline, buffer solution and acidic media. In alkaline medium, we found that complex **2** exhibited impressive electrocatalytic HER activity and produced a current density of -10 mA cm^{-2} at an overpotential of 260 mV, whereas complex **1** produced same current density at an overpotential of 334 mV. The electrochemical impedance spectroscopy (EIS) spectral study revealed the faster charge transfer kinetics of complex **2** than that of complex **1**. Similarly, the low Tafel slope (100 mV dec^{-1}) for the HER with complex **2** indicates faster HER kinetics compared to complex **1.** The chronoamperometric study showed that the complex **2** is stable

under electrocatalytic HER conditions for 5 h without losing the initial current density and it has also been established that complex structure retained after electrocatalysis.

Introduction

The abundance, elemental composition as well as nontoxicity of water make it an attractive "green" medium for sustainable energy storage processes.[1] H_2 has been identified as clean and renewable fuel with exceptionally high energy density (~142 MJ/kg).[2] The production of H_2 by electrochemical water splitting represents a viable option for moving towards carbon-free energy and justifying the environmental effects associated with greenhouse gas emissions.[3] In this respect, suitable electrocatalysts are required to lower the kinetic barrier and speed up the overall water-splitting process.[4, 5] Although the high rate of electrocatalytic H_2 evolution has been achieved using precious-metal-based electrocatalysts, their wide applications are limited due to low abundance and high cost.[3] Alternatively, earth-abundant 3d transition metal-based complexes have been developed as catalysts for water splitting.[6, 7] The use of molecular complexes is particularly appealing for hydrogen production because of the well-defined molecular structure and tunable electronic properties. Hence, it is possible to systematically tune the catalytic activity *via* rational ligand design based on mechanistic insights. Another added advantage of using a molecular complex is the immobilization of it on the electrode surface by ligand modification. Though metallic cobalt does not play any role in biological hydrogen production, its complexes have widely been explored for the electrochemical and photocatalytic H_2 evolution reaction.[8] In particular, cobalt complexes with planar (pseudo)macrocyclic ligands have been reported for electro- -as well as photocatalytic H_2 evolution reactions.[9-14] Cobaloxime complexes have also been utilized as molecular catalysts for electro- and photocatalytic production of H_2.[7, 8, 15, 16, 17] The benefits of using cobaloximes in H_2 production are associated with their easy and reproducible synthesis, stability toward O_2, and H_2 production activity at a relatively low overpotential. It has also been observed that the electronic properties of cobaloximes can be modulated by employing different substituents at the equatorial dioximes and/or axial ligands and therefore, the catalytic activity can easily be modified.[18, 19]

The immobilization of molecular catalysts onto conductive or semiconducting surfaces has emerged as a promising strategy for electrocatalytic hydrogen evolution reaction (HER) to attain the advantages of both homogeneous and heterogeneous catalytic systems.[8, 20-25] A high specific surface area, good electrical conductivity, and electrochemical stability of the conductive support may result in improved electrocatalytic activity.[26-29] The immobilization

also provides stability of the catalyst and thorough catalytic investigation delivers a deeper understanding of the mechanism together with redox events involved in the catalytic reactions.[30] There have been few reports, which utilize the noncovalent grafting strategy to immobilize cobaloxime derivatives onto the surface of carbon-based conducting surfaces for electrocatalytic H_2 evolution.[20, 31] Vincent Artero et al. displayed the diimine–dioxime cobalt catalyst immobilized on the surface of a carbon nanotube electrode.[13] The resulting electrocatalytic cathode material mediates H_2 generation with 55,000 turnovers in seven hours from fully aqueous solutions at low-to-medium overpotentials. In order to immobilize cobaloxime complex on to the surface of carbon cloth, Haining Tian et al. successfully grafted to fullerene derivative via 'click' chemistry, which was then used to modify carbon cloth electrode for both electro-catalytic and light driven water reduction. This hybrid material exhibited efficient hydrogen evolution activity, and a constant catalytic current of 2.7 mA cm^{-2} is reached at -0.8 V vs. NHE in bulk electrolysis experiment.[31] Later on Erwin Reisner and co-workers reported the copolymer-embedded cobaloxime integrated into a multiwall carbon nanotube matrix by π–π interactions. The polymeric hybrid material displays a catalytic activity four times higher and twice as long compared to its monomeric counterpart.[20]

For the water splitting, coupling of the cathodic proton reduction and anodic water oxidation in a single electrolyte solution is crucial to minimize the energy loss of the overall process.[32, 33] The water oxidation in the acidic medium is critical due to the stability and poor performance of the catalyst.[34, 35] Previous reports described the HER using cobaloxime complexes in the acidic and neutral media.[7, 36] Therefore, designing a hydrogen evolution catalyst for the alkaline medium is much more challenging to attain high efficiency in the overall water splitting as the reaction kinetics usually get slower as a result of added steps in the dissociation of water.[37]

Herein, we have synthesized two cobaloxime complexes containing N-(4-pyridylmethyl)-1,8-naphthalamide as one of the axial donor ligands (Scheme 1). Since, 1,8-naphthalimide functionality is redox active and it can influence the redox behaviour of the cobaloxime complexes improving the catalytic performance than the analogous pyridine complex. The immobilization of cobaloxime complexes onto the surface of activated carbon cloth (CC) produces complex@CC functional electrocatalysts for H_2 evolution. To the best of our knowledge, this is the rare study of electrochemical HER using cobaloxime complexes as a molecular catalyst in an alkaline medium. We have also compared the results with analogous studies in buffer solution as well as acidic media. However, complexes showed enhanced

HER activity in the alkaline medium compared to the acidic and buffer solutions. Complex **2** attained a current density of -10 mA cm^{-2} at only 260 mV overpotential lower than that of complex **1** in the alkaline medium. Moreover, the lower Tafel slope and charge transfer resistance was also recorded for complex **2**.

Results and discussion

Molecular cobaloximes (**1** and **2**) were synthesized by dissolving $CoCl_2.6H_2O$, dimethylglyoxime (two equivalents), and NaOH in 95% ethanol at 70 °C followed by the addition of one equivalent of N-(4-pyridylmethyl)-1,8-naphthalamide ligands (Scheme 1).[38] Cobaloximes are soluble in common organic solvents (dichloromethane, DMSO, chloroform, and DMF) and insoluble in water and methanol.

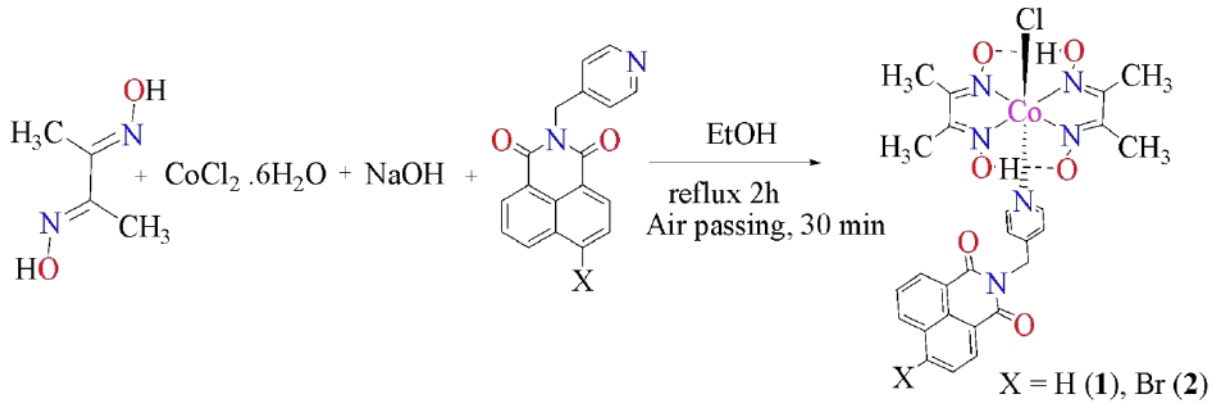

Scheme 1. Synthetic methodology for complexes **1- 2**

The axial pyridyl ligands [N-(4-pyridylmethyl)-1,8-naphthalamide (L_1 and L_2)] were synthesized according to the literature procedure using 1,8-naphthanhydride derivatives and 4-pyridinemethylamine.[39, 40] We have introduced Br at 4-position of 1,8-naphthalimide unit of axial pyridine ligand in order to see the effect of substituent on the electrocatalytic activity. Since, 1,8-naphthalimide functionality is redox active group and hence this may alter the electronic property of the catalyst resulting in a better catalyst than analogous pyridine complex.

Both cobaloxime complexes are well characterized by ^1H and $^{13}C\{^1H\}$ NMR, FT-IR and UV-Vis spectral analyses (Fig. S1-S10, ESI†). Furthermore, the solid-state structures of both complexes (**1-2**) have also been determined by single crystal X-ray crystallography (SCXRD). The UV-Vis absorption spectra exhibited the salient features of the intra ligand π–

π* charge transfer band and ligand to metal charge transfer (LMCT) band in the region of ~230-360 nm. The *d-d* transition band appeared at ~500 nm for both complexes (Fig. 1)**,** which suggests the ligation of axial pyridyl ligands N-(4-pyridylmethyl)-1,8-naphthalamide to the cobalt center.[36] The FT-IR spectral studies of complexes **1**-**2** showed a strong signal at ~1700 cm^{-1} attributed to the stretching of CO functional group ($\nu_{C=O}$) and the absorption band around ~3400-3500 cm^{-1} represents the O–H stretching frequency ($\nu_{O\cdots H-O}$) (Fig. S1 and S2, ESI†). The absorption bands around ~500-550 cm^{-1} are the characteristics of Co–N and Co–Cl functional groups of cobaloxime complexes.[41]

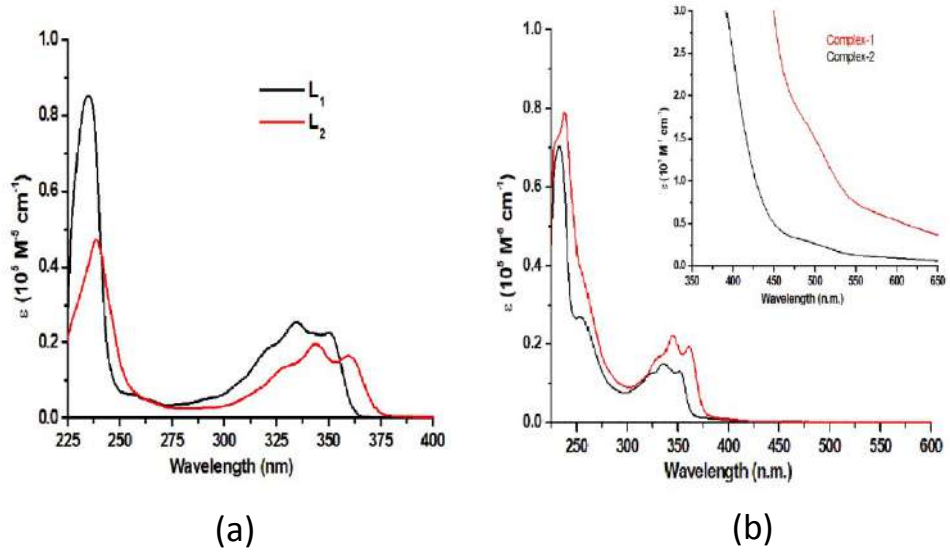

Fig. 1 (a): UV-Vis spectra of ligands L_1 and L_2 (b) Complexes **1** and **2** in CH_2Cl_2 solution at 10^{-5} molar concentration; inset shows at 10^{-1} molar concentration.

The diamagnetic nature of cobaloximes allowed us to characterize both cobaloxime complexes by NMR spectral studies. The ^1H and $^{13}C\{^1H\}$ NMR spectral data for complexes are provided in the Experimental Section. The NMR peaks were consistent with the molecular formulae proposed in Scheme 1. The pyα protons resonance signal was observed as a doublet in ^1H NMR spectra at chemical shift 8.14 ppm in **1** and **2**, which is approximate ~0.40 ppm upfield shifted as compared to the uncoordinated ligands (δ ~8.54 ppm)**.** Similarly**,** an upfield shift (0.18 ppm) was observed for py_β protons and the signal for these protons appeared at ~7.18 ppm. It has been shown that the presence of dmgH as an equatorial ligand in the cobaloximes causes an upfield shifting of axially coordinated pyridine protons due to the enhanced shielding effect of the ring current in the metallabicycle.[42, 43] The resonance signals for methyl protons of $dmgH_2$ ligand in **1** and **2** appeared as a singlet at 2.39 and 2.37 ppm which are shifted downfield (~0.45 ppm) with respect to uncoordinated $dmgH_2$

ligand (δ 1.91 ppm). The $^{13}C\{^1H\}$ NMR spectra of complexes **1** and **2** showed downfield shifted (~4 ppm) of methyl carbons of dmgH ligand as compared to uncoordinated $dmgH_2$ and appeared at 13.25 and 13.02 ppm, respectively.

The phase purity of the bulk samples of cobaloximes **1** and **2** was confirmed by comparing the experimental PXRD patterns with the respective simulated powder patterns obtained from the single-crystal X-ray diffraction (SCXRD) data. Both the PXRD patterns (experimental and simulated) match well indicating the phase purity of the bulk samples (Fig. S11 and S12, ESI†).

Description of Single Crystal X-ray Structures

The solid state structures of complexes **1** and **2** have been determined by single crystal X-ray diffraction studies. Single crystals suitable for X-ray analysis were grown upon slow evaporation of DCM/DMF solution of the complexes within 3-4 weeks. Crystallographic data of both complexes and their structure refinement details are presented in Table 1. The molecular structures are presented in the Fig. 1 and the selected bond lengths and angles are given in the Table 2.

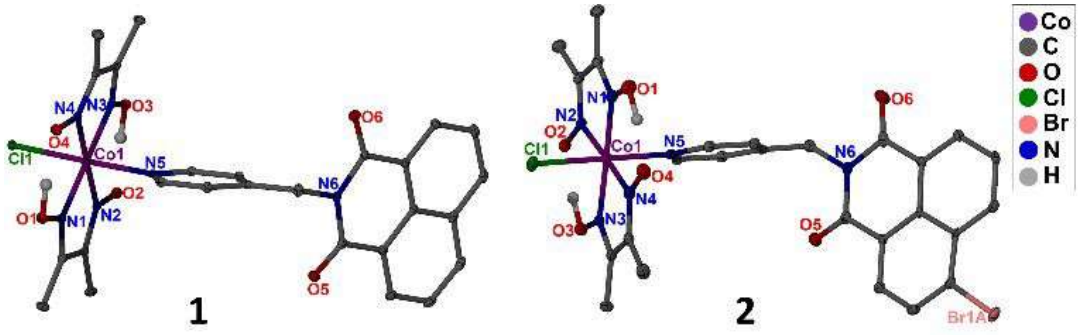

Fig. 1 Molecular structures of **1** and **2** with ellipsoids at 30% probability showing the atom-numbering except for carbon atoms. Aromatic, methylene, and methyl hydrogen atoms are omitted for clarity. For complex **2** only the major fractions are shown in the figure.

Table 1: Crystal data and structure refinement parameters for cobaloximes **1** and **2**.

Identification code	**1**	**2**
Empirical formula	$C_{26}H_{26}ClCoN_6O_6$	$C_{26}H_{25}BrClCoN_6O_6$
Formula weight	612.91	691.81
Temperature/K	100(2)	100(2)
Crystal system	monoclinic	monoclinic
Space group	P 21/c	P 21/n
a/Å	7.9318(7)	9.1696(4)
b/Å	15.0107(14)	14.6019(6)
c/Å	22.6228(19)	21.0020(8)

View Article Online
DOI: 10.1039/D2DT02511F

α/°	90	90
β/°	93.569(3)	101.5130(10)
γ/°	90	90
Volume/Å^3	2688.3(4)	2755.5(2)
Z	4	4
ρ_{calc}g/cm^3	1.514	1.668
μ/mm^{-1}	0.791	2.223
F(000)	1264.0	1400
Crystal size/mm^3	0.23 × 0.19 × 0.15	0.21 × 0.18 × 0.12
Radiation	MoKα (λ =0.71073)	MoKα (λ =0.71073)
2Θ range for data collection/°	5.72 to 56.628	5.324 to 56.588
Index ranges	$-10 \le h \le 10$ $-20 \le k \le 20$ $-30 \le l \le 30$	$-12 \le h \le 12$ $-19 \le k \le 19$ $-27 \le l \le 27$
Reflections collected	9973	9948
Independent reflections	6691	6822
Data/restraints/parameters	6691/0/367	6822/0/420
Goodness-of-fit on F^2	1.035	1.105
Final R indexes [I>2σ (I)]	5547	6027
Final indices[I>2σ(I)] R_1[a], wR_2[b]	0.0352, 0.0796	0.0481, 0.1229
$R_{1[a]}$, $wR_{2[b]}$ [all data]	0.0486, 0.0883	0.0560, 0.1274
Residual electron Density, e/Å-3	0.41/-0.46	0.84/-1.33
CCDC	2163937	2163938

Complexes **1** and **2** crystallize in the monoclinic system with $P2_1/c$ and $P2_1/n$ space group respectively. The molecular structures of both complexes indicated that the central cobalt atom is in distorted octahedral geometry with four nitrogen atoms of the dioxime in the equatorial plane and axial sites are occupied by Cl and pyridyl-N of ligands $\mathbf{L_1}$ and $\mathbf{L_2}$ (Fig. 1). The Co–Cl and Co–N(py) bond distances (Co1–Cl1 [2.233(1), 2.233(1)], Co1–N5 [1.957(2), 1.965(3)]) of complexes **1** and **2** are comparable with the bond distances reported in the literature for the similar cobaloximes $ClCo(dmgH)_2Py$.[44] Due to flexibility, $Co(dmgH)_2$ unit undergoes geometrical deformation in both complexes and deviation of the cobalt atom from the mean equatorial N4 plane are -0.008 and +0.034 Å, respectively. A negative sign indicates that the deviation is toward the axial Cl group and bending of dioxime units toward pyridine nitrogen whereas positive sign indicates that the deviation is toward the axial pyridine nitrogen and bending of dioxime units is toward axial Cl. It was observed that in the case of bromide substituted complexes **2,** the bromo-1,8-naphthalimide unit is disordered over two positions.

It is interesting to note that the a closer inspection of solid-state structure of complex **1** reveals a number of weaker intermolecular non-covalent interactions such as C–H···O, C–H···Cl, and C–H···π (Centroid) leading to the formation of dimeric as well as 1D supramolecular structures (Figs. 2-4).

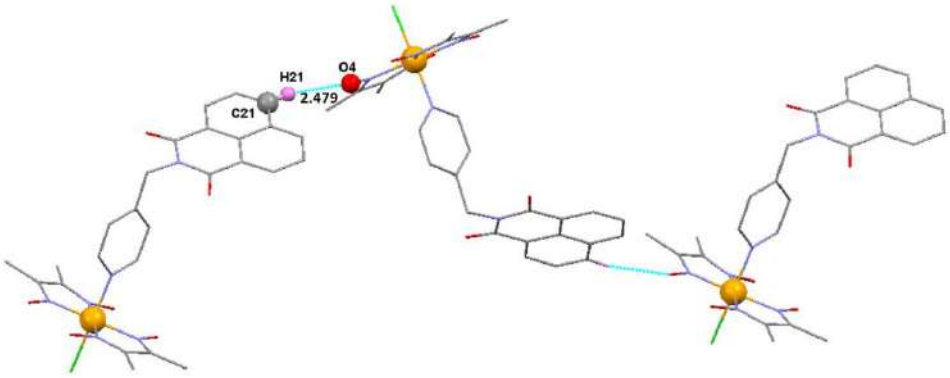

Fig. 2 Hydrogen bonded 1-D polymeric network of complex **1** sustained by C–H···O interactions.

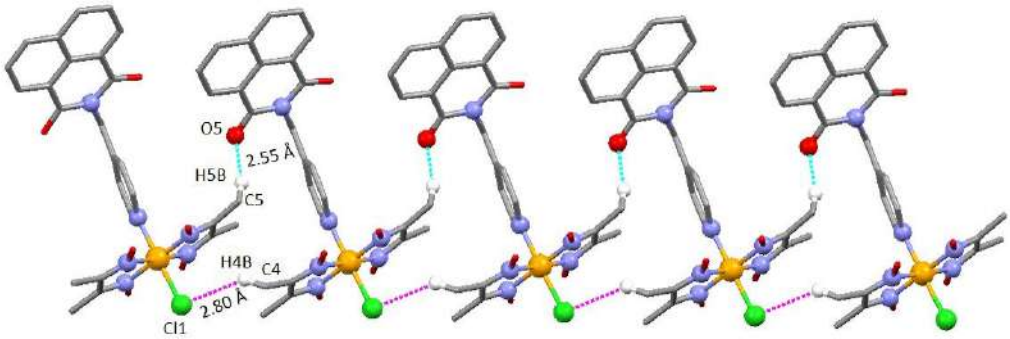

Fig. 3 Hydrogen bonded 1D polymeric network of complex **1** sustained by C–H···O and C–H···Cl interactions.

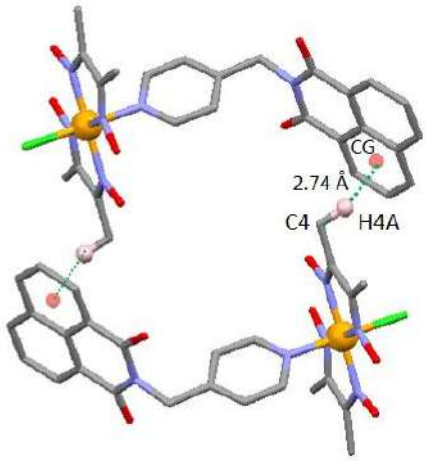

Fig. 4 Hydrogen bonded dimeric unit of complex **1** sustained by C–H···π interaction.

View Article Online
DOI: 10.1039/D2DT02511F

Similarly, complex **2** also exhibits weak non covalent intermolecular interactions (C–H···O, C-H···Br and C-H···π) resulting in the formation of 1D supramolecular structure and also dimeric unit (Figs. 5 and 6). Dimensions of these weak interactions are given in Table 3 and 4.

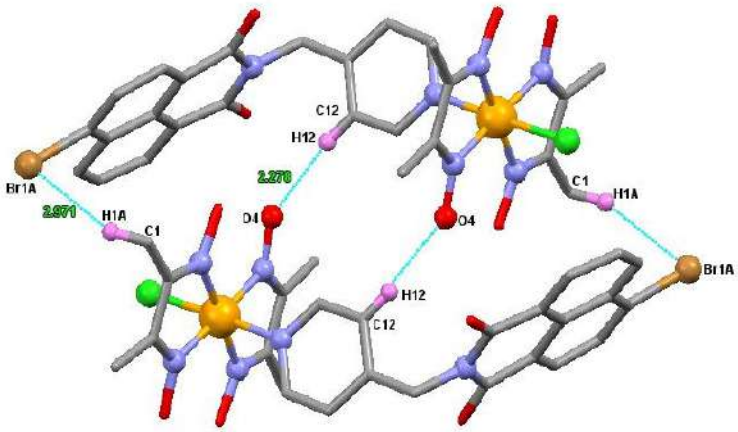

Fig. 5 Hydrogen bonded dimeric structure of complex **2** sustained by C–H···O and C–H···Br interactions.

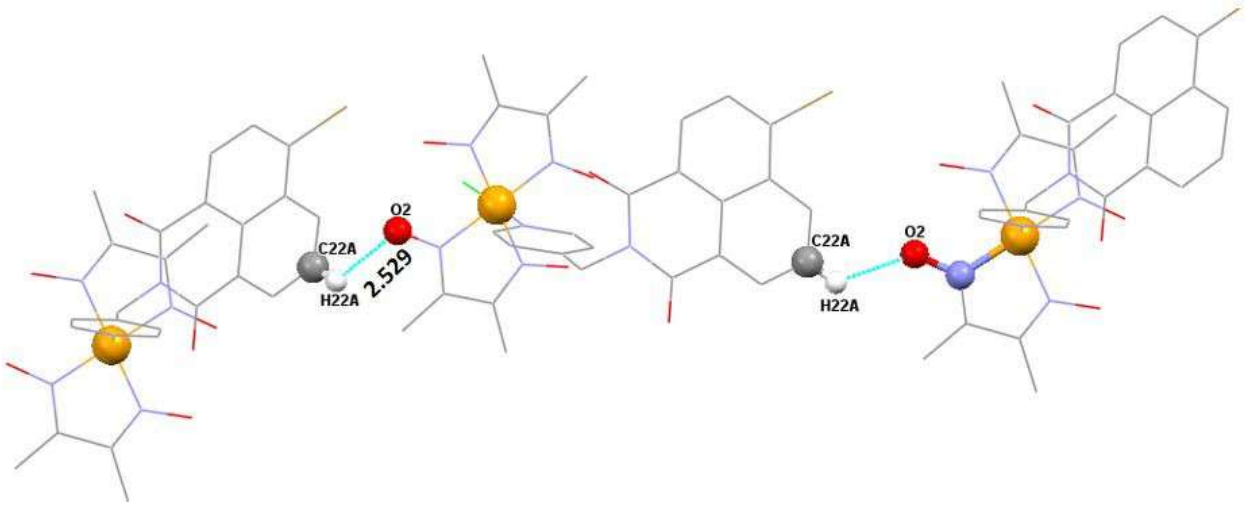

Fig. 6 Hydrogen bonded 1-D polymeric network of complex **2** sustained by C–H···O interactions.

Table 2: Selected bond lengths (Å) and bond angles (°) in complexes **1** and **2**.

Bond distances(Å)	**1**	**2**
Co1–N1	1.8995(15)	1.894(3)
Co1–N2	1.8986(15)	1.898(2)
Co1–N3	1.8881(15)	1.889(3)
Co1–N4	1.8907(16)	1.904(3)

View Article Online
DOI: 10.1039/D2DT02511F

Co1–N5	1.9573(16)	1.965(3)
Co1–Cl1	2.2337(5)	2.2333(9)
Bond Angles(°)		
N2–Co1–N1	81.19(7)	81.30(11)
N3–Co1–N4	81.94(7)	81.38(12)
N4–Co1–N1	98.54(7)	98.27(11)
N3–Co1–N2	98.34(7)	98.98(11)
N5–Co1–Cl1	178.64(5)	177.82(7)

Table 3: List of non-bonding intermolecular interactions of complexes **1** and **2.**

Complex	**D-H···A**	**D-H (Å)**	**H···A (Å)**	**D···A (Å)**	**D-H···A (°)**
1	C21-H21···O4	0.95	2.48	3.38	157.88
1	C5-H5B···O5	0.98	2.55	3.52	167.84
2	C12-H12···O4	0.95	2.28	3.20	164.20
2	C22A-H22A···O4	0.95	2.53	3.18	125.59
	C-H···Cl	**C-H (Å)**	**H···Cl (Å)**	**C···Cl (Å)**	**C-H···Cl (°)**
1	C4-H4B···Cl1	0.98	2.80	3.564	134.61
	C-H···Br	**C-H (Å)**	**H···Br (Å)**	**C···Br (Å)**	**C-H···Br (°)**
2	C1-H1A···Br1A	0.98	2.97	3.87	153.04

Table 4: List of non-bonding intermolecular C-H···π interactions of complex **1**

Complex	**C–H···π**	**distance C–H···π (Å)**
1	C4-H4A···π(C16-C20, C25)	2.742

Electrocatalytic Hydrogen Evolution Reaction (HER) Activities of Complexes 1 and 2

After the successful synthesis and characterization of complexes (**1-2)**, these complexes were immobilized on the surface of carbon cloth (CC) in order to study their electrochemical behavior. The complexes@CC were then used as the working electrode for electrochemical hydrogen evolution reactions.

The linear sweep voltammetry (LSV) was recorded in acidic (pH 0.13), phosphate buffer (pH 6.61), and alkaline media (pH 13.8) to investigate the HER activity of the complexes. In 0.5 M H_2SO_4 solution (pH 0.13), complex **1** delivered -10 mA cm^{-2} current density at 435 mV overpotential for HER (Fig. S13, ESI†) while complex **2** attained the same current density at 409 mV overpotential. Under similar reaction conditions, the bare CC electrode produces -10 mA cm^{-2} current density at 465 mV overpotential. Further, the HER activity of complexes **1**

and **2** was also evaluated in the phosphate buffer (pH 6.61) (Fig. S14, ESI†). In this solution, complexes **1** and **2** also showed enhanced hydrogen evolution activity compared to the bare CC. Complex **1** attained -1.0 mA cm^{-2} current density at 420 mV overpotential while the improved HER performance was recorded for complex **2** at only 295 mV overpotential delivering the same current density.

We have also investigated the electrocatalytic HER performance of complexes **1** and **2** in 1.0 M aqueous KOH solution (pH 13.8) (Fig. 7a). In alkaline medium, complex **1** reached the cathodic current density of -10 mA cm^{-2} at an overpotential of 334 mV while complex **2** showed enhanced HER activity to attain the same current density merely at 260 mV overpotential. As the improved HER activity for complexes **1** and **2** was recorded in the alkaline solution, further electrochemical characterizations were performed in the same medium.

The HER activity of complexes **1** and **2** were also compared with $[ClCo(dmgH)_2Py]$ and bare CC (Figs. S15 and S16, ESI†). The polarization curves revealed that $[ClCo(dmgH)_2Py]$ requires 370 mV overpotential for -10 mA cm^{-2} current density, which was higher than that of complexes **1** and **2**. The results indicated an excellent HER activity of complexes **1** and **2** compared to the $[ClCo(dmgH)_2Py]$ in an alkaline medium. It is well established that the electron-donating group at the 4-position of axial pyridine increases the electrocatalytic activity by increasing the basicity at Co center.[12, 45, 46] A similar observation is found in this study as well, where the 1,8-naphthalimide unit is attached at 4-position of axial pyridine ligand in both complexes **1** and **2**. In addition, the HER activity of the complexes was also found to be better/comparable to the previously reported cobaloxime based electrocatalysts used for HER (Table S1, ESI†).

In the alkaline medium, the difference in the catalytic activities of complexes are observed due to the variation in the electronic environment around the cobalt center induced by the different structural and electronic properties of the peripheral ligands. The short CV profile of complexes **1** and **2** revealed the redox peak (R_1 and R_2) for the reduction of Co(II) to low valent Co(I) (Fig. 7b).[47, 48] The peak R_1 for the reduction of Co(II) to Co(I) in complex **1** was observed at the -220 mV overpotential while the reduction peak R_2 in complex **2** was found at -146 mV overpotential (Fig. 7b).

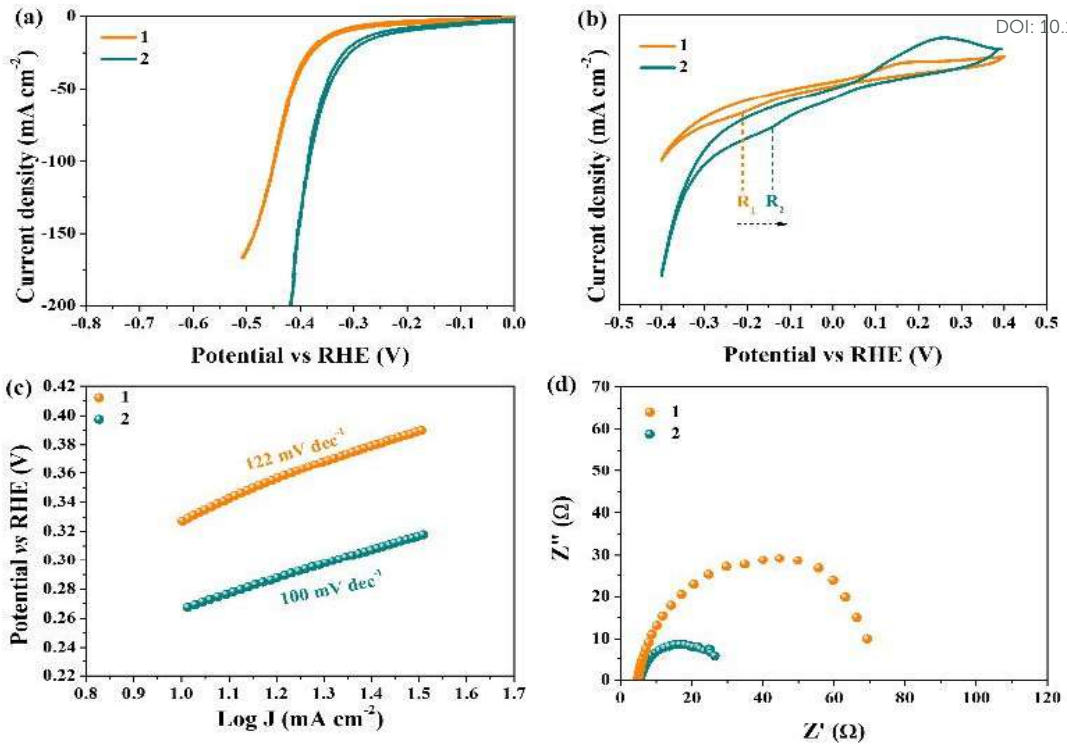

Fig. 7. (a) CV profiles for the hydrogen evolution reaction (HER) of complexes **1** and **2** in 1.0 M aqueous KOH solution (pH 13.8) at room temperature; (b) short CV profiles during the HER of complexes **1** and **2** showing the redox peak for the Co(II)/Co(I) redox couple; (c) Tafel plots of complexes **1** and **2** showing the lowest Tafel slope value for complex **2**; and (d) EIS spectra of complexes **1** and **2** showing the lowest charge transfer resistance for complex **2**.

The R_2 peak for the reduction of Co(II) to Co(I) in complex **2** was shifted negatively at the lower potential compared to complex **1**, which was attributed to the change of the electronic environment around the Co-center.[47,48] Therefore, facile reduction of Co(II) to Co(I) was observed in complex **2** at lower potential promoting the higher HER activity as compared to complex **1**. The comparison of the short CV profiles of **1** and **2** with [ClCo(dmgH)$_2$Py] also indicated the higher potential is required for the reduction of Co(II) to Co(I) in [ClCo(dmgH)$_2$Py] as compared to complex **2** (Fig. S16, ESI†). It is interesting to note that the substitution of hydrogen with Br at 4-position of 1,8-naphthalimide unit of axial pyridine ligand in complex **2** enhances the catalytic activity for HER. The substitution of hydrogen with Br in complex **2** may be resulted the increment of the electron density due to the delocalization of the lone pair of electrons of Br into the naphthalimide ring through resonance (complex **1** versus **2**). We have immobilized NDI ligands also on carbon cloth and carried out the cyclic voltammetry in 1.0 M KOH solution. Interestingly, we were able to

View Article Online
DOI: 10.1039/D2DT02511F

detect the redox peaks for Co(II) to Co(I) and also NDI ligand centered reduction in the complex **2** while only one redox peak was detected in free NDI ligand (Fig. S17, ESI†).[42-43]

To get more insight about the redox properties, the CV of complex **2** and the corresponding axial NDI ligand was carried out in acetonitrile. In the CV profile of complex **2**, the peaks for the reduction of Co(III) to Co(II) and Co(II) to Co(I) were detected (Fig. S18, ESI†) while NDI ligand exhibited two reduction peaks, which may be attributed to the generation of $NDI^{\bullet-}$ and NDI^{2-} (Fig. S18, ESI†).

For the complex **2**, the reduction peak current density against the scan rate was plotted (Figs. S19 and S20, ESI†). Linear plot clearly shows that there is no mass transfer limitation in the solution. Further, we have also carried out the scan rate dependent CV after immobilizing the complex **2** on carbon cloth in 1.0 M aqueous KOH solution (Fig. S21a, ESI†). Interestingly, the plot has shown the linearity, indicating the minimum mass transfer limitation when supported on carbon cloth (Fig. S21b, ESI†).

Further to get more insight about the excellent HER activity of the complexes, the surface concentration of electroactive Co sites was determined by the reduction peak area integration method (Fig. S22, ESI†).[49,50] Firstly, the surface concentration of electroactive species of the complexes **1**, **2** and $[ClCo(dmgH)_2Py]$ was calculated using the Sharp equation (Equation S2 ESI).[49,50] The peak current under the CV is related to the surface concentration of electroactive species. The surface concentration of the electroactive species were calculated to be 1.48 x 10^{-5} mol cm^{-2} for complex **2**, 0.38 x 10^{-5} mol cm^{-2} for $[ClCo(dmgH)_2Py]$, and 1.05 x 10^{-5} mol cm^{-2} for complex **1**. The HER activity of the complexes was also normalized with the surface concentration of electroactive sites. Even after normalization the complex **2** showed enhanced HER activity among the studied catalysts (Fig. S23, ESI†).

To establish the hypotheses, the charge transfer kinetics of the synthesized complexes were evaluated by electrochemical impedance spectroscopy (EIS). The EIS spectra revealed the lower radius of the semi-circle for complex **2** as compared to complex **1** (Fig. 7d). The R_{ct} value for complex **2** was determined to be 21.24 Ω, lower than that of complex **1** (63.95 Ω). The results suggested the faster charge transfer kinetics of complex **2** than that of complex **1**.

Further, the HER kinetics of the synthesized complexes were determined from the Tafel plots. Complex **2** showed the lowest Tafel slope value (100 mV dec^{-1}), indicating faster HER kinetics as compared to complex **1** (Fig. 7c). The Tafel slopes have revealed that the Volmer step ($H_2O + e^- \rightarrow H_{ads} + OH^-$) is the followed by the complex **2,** which involved the water dissociation as the rate determining step.[51, 52]

The stability of complex **2** under HER condition i.e. 1 M aqueous KOH was studied by chronoamperometric measurement. Interestingly, this study showed the stability of complex **2** for 5 h without losing the initial current density (Fig. S24, ESI†). We have performed the cyclic stability of the complex **2** immobilized on carbon cloth under cyclic voltammetric conditions. We have observed that the complex **2** exhibited excellent stability of 500 CV cycles as no change in the current density and overpotential have been recorded (Fig. S25, ESI†).

Further, the faradaic efficiency of complex **2** was determined using a separated two compartment H-type cell by the gas displacement method. Interestingly, faradaic efficiency was determined to be ~98.6% indicating the excellent performance of complex **2** for hydrogen evolution (Fig. S26, ESI†). [53-55]

Therefore, we conclude that the improved electrochemical HER activity of complex **2** in the alkaline medium can be attributed to its unique structural and electronic properties, which resulted in (i) the facile reduction of Co(II) to Co(I) at a lower potential, (ii) increment in the basicity around Co centers due to the electron-donating methyl group, as well as Br substituent in the axial pyridyl ligand, (iii) the low charge transfer resistance, and (iv) optimized binding energy for the protons. Although the HER activity of complex **2** was found to be better than complex **1** in acidic, buffer, and alkaline medium, the best activity of both complexes was recorded in alkaline medium.

The retention of the molecular entity is a matter of concern during the electrocatalytic HER.[56] The complex may retain its entity or it can react with KOH destroying its ligand structure to form cobalt hydroxide. To ascertain this, we have recorded UV-vis and ^{1}H NMR spectra of complex after HER electrocatalysis. Interestingly, UV-vis and ^{1}H NMR spectra of complex **2** recovered after the electrocatalysis showed a negligible change in the signals and peak positions (Fig. S27-S29, ESI†). This result indicated that complex **2** is stable and retained its molecular entity under electrocatalytic conditions. We have also carried out scanning electron microscopy (SEM) and energy dispersive X-ray spectroscopy (EDX) to determine the surface properties. SEM images indicated that the morphology of the complex **2** was not changed after the 5 h chronoamperometric HER (Fig. S30, ESI†). EDX studies revealed that the elemental composition of the complex **2** was almost similar before and after the catalysis (Fig. S31, ESI†). These results further confirmed the stability of molecular entity of complex **2**.

View Article Online
DOI: 10.1039/D2DT02511F

Experimental Section

Material and methods

All reactions were carried out in the open air and at room temperature unless specifically mentioned. Solvents were purified by standard procedures and dried before use according to the requirements.[57] All of the commercially available reagents of analytical grade were purchased from (Sigma-Aldrich), and were used as received without further purification. Melting points of the complexes were determined in open capillaries with a Gallenkamp apparatus and are uncorrected. FT-IR spectra in the 4000-400 cm^{-1} region were recorded as KBr disks using a PerkinElmer FT-IR spectrophotometer. ^{1}H and $^{13}C\{^{1}H\}$ NMR spectra were obtained either in DMSO-d_6 or $CDCl_3$ on a JEOL ECZ500 MHz NMR spectrometer. Tetramethylsilane (TMS) was used as an internal standard for recording NMR spectra. UV-visible absorption spectra in solution (CH_2Cl_2) state were obtained on a Shimadzu UV-1800 instrument. The N-(4-pyridylmethyl)-1,8-naphthalamide derivatives (**L_1** and **L_2**) were synthesized according to the literature procedure.[39, 40]

Synthesis of N-(4-pyridylmethyl)-1,8-naphthalamide derivatives (L_1 and L_2)

Synthesis of Ligand L_1

Ligand **L_1** was synthesized by condensation reaction between 4-aminomethyl pyridine (0.545 g, 5 mmol) and 1,8-naphthalic anhydride (1 g, 5 mmol) in methanol. In this reaction, 1,8-naphthalic anhydride (5 mmol) was taken in methanol (20 mL) and 4-aminomethyl pyridine (0.545g, 5 mmol) was added in the presence of 2 drops of triethyl amine as the catalyst. The reaction mixture was refluxed for 3 h and then cooled at room temperature. A white color solid was separated out, which was filtered, washed with methanol (4 x 5 mL) and dried under a vacuum. Yield: 1.3 g (~90%). ^{1}H NMR (500 MHz, $CDCl_3$): δ 8.61 (d, 2H, J = 7 Hz), 8.53 (d, 2H, J = 5 Hz), 8.23 (d, 2H, J = 8.5 Hz), 7.77 (t, 2H, J = 14.5 Hz), 7.37 (d, 2H, J = 6 Hz), 5.37 (s, 2H, CH_2), $^{13}C\{^{1}H\}$ NMR ($CDCl_3$, 125 MHz): δ 164.35, 150.26, 146.18, 134.69, 131.95, 128.48, 127.32, 123.50, 122.51, 42.89.

Synthesis of Ligand L_2

Ligand **L_2** was synthesized following the procedure as described for the synthesis of L_1 from 4-Br-1,8-naphthalic anhydride (300 mg, 1 mmol) and 4-aminomethyl pyridine (117 mg, 1 mmol) in 10 mL methanol. Product was obtained as pale yellow solid. Yield:150 mg (~41%). ^{1}H NMR (500 MHz, $CDCl_3$): δ 5.35 (s, 2H), 8.67 (d, J = 7.5 Hz, 1H), 8.60 (d, J = 8.5 Hz,

1H), 8.54 (d, J = 5 Hz, 2H), 8.43 (d, J = 8 Hz, 1H), 8.06 (d, J = 7.5 Hz, 1H), 7.86 (t, J = 16 Hz, 1H), 7.36 (d, J = 5 Hz, 2H), $^{13}C\{^{1}H\}$ NMR ($CDCl_3$, 125 MHz): δ 163.44, 149.94, 145.50, 133.69, 132.41, 131.56, 131.51, 130.79, 130.65, 128.96, 128.10, 123.15, 122.58, 121.69, 42.61.

General Synthetic Procedure of Cobaloximes [ClCo(dioxime)$_2$L] (1 and 2)

Cobaloxime complexes were synthesized by modifying the earlier literature procedure.[38] $CoCl_2.6H_2O$ (0.5 mmol), dimethylglyoxime (1 mmol) and NaOH (0.5 mmol) were dissolved in 95% ethanol and heated to 70 °C. Pyridyl ligand {N-(4-pyridylmethyl)-1, 8-naphthalamide (0.5 mmol) was then added and stirred for 1 h. The resulting solution was cooled to room temperature followed by the passing of a stream of air through the solution for 30 min. This resulted in the precipitation of a brown solid. The solid precipitate was filtered and successively washed with water, ethanol, and diethyl ether. Cobaloxime complexes were obtained as brown solid and these were crystallized in DCM/DMF (8:2).

Yield of **1:** 0.180 g (~70%), Mp: 260 °C, FT-IR (KBr, cm^{-1}): ν = 3442 (ν_{O-H}), 3044 ($\nu_{=C-H}$), 2990 (ν_{-C-H}), 1700 ($\nu_{C=O}$, carboxylate), 1567 ($\nu_{C=N}$, dmgH), 1235 (ν_{N-O}). ^{1}H NMR (500 MHz, $CDCl_3$): δ 8.60 (d, J = 7 Hz, 2H), 8.30 (d, J = 8 Hz, 2H), 8.14 (d, J = 4 Hz, 2H), 7.81 (t, J = 15 Hz, 2H), 7.19 (d, J = 4 Hz, 2H) 5.32(s, 2H), 2.39 (s, 12H). $^{13}C\{^{1}H\}$ NMR (125 MHz, $CDCl_3$): δ 164.21, 152.74, 151.04, 150.01, 135.19, 132.15, 131.88, 128.35, 127.40, 124.39, 121.85, 42.11, 13.25.

Yield of **2:** 0.195 g (~67%), Mp: 220 °C, FT-IR (KBr, cm^{-1}): ν = 3409 (ν_{O-H}), 3059 ($\nu_{=C-H}$), 2924 (ν_{-C-H}), 1707 ($\nu_{C=O}$, carboxylate), 1568 ($\nu_{C=N}$, dmgH), 1236 (ν_{N-O}). ^{1}H NMR (500 MHz, $CDCl_3$): δ 8.66 (d, J = 5 Hz, 1H), 8.65 (d, J = 5 Hz, 1H), 8.40 (d, J = 10 Hz, 1H), 8.14 (d, J = 10 Hz, 2H), 8.09 (d, J = 7.5 Hz, 1H), 7.89 (t, J = 7.5 Hz, 1H), 7.18 (d, J = 5Hz, 2H), 5.30 (s, 2H), 2.37 (s, 12H). $^{13}C\{^{1}H\}$ NMR (125 MHz, $CDCl_3$): δ 163.39, 152.59, 150.85, 149.48, 134.30, 132.69, 131.80, 131.51, 131.33, 130.78, 128.93, 128.27, 124.18, 122.04, 121.11, 41.96, 13.02.

Single Crystal X-ray Diffraction (SCXRD)

Single crystal X-ray diffraction data were collected on a Bruker APEX-III D8 Quest diffractometer equipped with an Oxford Cryosystems Cryostream 700Plus cryostat. A multilayer monochromator with MoKα radiation (λ = 0.71073 Å) from an Incoatec IμS microsource was used. Data reduction was carried out by means of standard procedures using the Bruker software package SAINT[58] and absorption corrections and the correction of other

View Article Online
DOI: 10.1039/D2DT02511F

systematic errors were performed using SADABS.[59, 60] The structures were solved by direct methods using SHELXS-97 and refined using SHELXL-97.[61] X-Seed[62] was used as the graphical interface for the SHELX program suite. Hydrogen atoms were placed in calculated positions using riding models. The bromo-1,8-naphthalimide unit in complex **2** is modelled using part command as it is disordered over two positions.

Fabrication of Complexes on Activated Carbon Cloth (CC)

Complex (3 mg) was dissolved in 50 μL of dichloromethane followed by the addition of 10 μL ethanolic 0.05 wt% Nafion solution and this mixture was sonicated for 2 min. Subsequently, the mixture was drop casted on the activated carbon cloth (CC).

Electrochemical Measurements

Electrochemical HER experiments were performed under heterogeneous condition in a single-compartment three-electrode electrochemical cell in basic (1.0 M aqueous KOH solution), buffer solution and acidic media (0.5 M H_2SO_4). Complex@CC was used as the working electrode and platinum wire as the counter electrode. Ag/AgCl electrode was used as the reference electrode and the applied potential was represented against reversible hydrogen electrode (RHE) by using the formula.[3, 63]

$$E(RHE) = E(Ag/AgCl) + 0.197 + 0.059pH$$

Corrections for iR losses and background current were included for all the CV and LSV measurements (70% iR compensation) whereas chronoamperometric data were represented without any iR correction.

All electrochemical experiments under homogeneous condition where perform in a three-neck single comportment electrochemical cell. All cyclic voltammetry was performed in acetonitrile (10 mL) containing 0.1 M $[NBu_4][PF_6]$ supporting electrolyte degassed with N_2 for 5 min. A glassy carbon electrode (2 mm diameter) was used as working electrode which was thoroughly cleaned prior to each measurement by polishing with wet alumina powder on a polishing pad, then washed with solvent. The counter electrode was a platinum wire and Ag/AgCl electrode was used as reference electrode.

Post Electro-catalytic Experiments

Since, it was very difficult to recover the catalyst from the surface of carbon cloth, we drop-casted catalysts onto the surface of FTO to easy recovery of catalyst for performing the post

electro-catalytic characterization. We deposited the catalyst on to the surface of FTO and the FTO was air dried for 15 min. This catalyst deposited FTO electrode was used as working electrode for electocatalysis experiment in 1.0 M KOH solution. After electrocatalysis, the FTO electrode was washed with distilled water for 2-3 times and air dried for 4 h. Further, the catalyst was collected from FTO surface for NMR and UV-Vis spectral analysis.

Conclusions

In summary, we have synthesized and characterized two new cobaloxime complexes containing N-(4-pyridylmethyl)-1,8-naphthalamide as one of the axial donor ligands. Single crystal X-ray structures indicated that complexes are discrete molecule with distorted octahedral geometry around central cobalt atom. Also, a close inspection of crystal structures showed the presence of weak non covalent interaction resulting formation of supramolecular structures. We have demonstrated that the immobilization of complexes onto the surface of carbon cloth produces a highly active and stable electrocatalyst for hydrogen evolution reaction in alkaline medium. The presence of 1,8-naphthalamide functionality at 4-position of axial pyridine ligand enhances the electro-catalytic HER activity in comparison to $[ClCo(dmgH)_2Py]$ catalyst. Although, the HER activities of complex **2** in acidic, buffer and alkaline media found to be better than complex **1**, both complexes exhibited best activity in alkaline medium. Complex **2** produces -10 mA/cm^{-2} current density at an overpotential of 260 mV in 1M KOH whereas complex **1** produces same current density at 334 mV. Electrochemical impedance spectroscopy (EIS) studies showed lower charge transfer resistance (21.24 Ω) and also low tafel slop (100 mV dec^{-1}) indicating faster charge transfer kinetics and faster HER kinetics respectively in complex **2**.The approach of synthesizing new cobaloximes containing the 1,8-naphthalamide group and their immobilization on carbon cloth surface could enable the development of new molecular electrocatalysts without using precious metals in the field of electrochemical water splitting.

Author contribution

The manuscript was written through contribution of all authors.

Supporting Information

FT-IR spectra and ^{1}H, $^{13}C\{^{1}H\}$ NMR spectra of ligands and complexes, PXRD of complexes, homogeneous and heterogeneous electrochemical CV and LSV profile, chronoamperometric measurement graph, SEM and EDX spectra of complex **2** (before and after the catalysis), CV

profile for the hydrogen evolution reaction, UV-Vis spectra of complex **2 (**After and before the catalysis).

AUTHOR INFORMATION

Corresponding Author

*Email: prem.lama@iip.res.in

*Email: arindam.chy@iitbhu.ac.in

*Email: kamlesh.kumar@bhu.ac.in

ORCID

N. Singh 0000-0003-1578-5456

A. Indra 0000-0002-8572-0423

K. Kumar 0000-0001-7374-5941

Conflicts of interest

There are no conflicts of interest to declare.

Acknowledgements

We gratefully acknowledge financial support from the University Grants Commission (UGC), New Delhi for the award of UGC-BSR Research Start-Up-Grant (No. F. 30-431/2018 (BSR)), Banaras Hindu University–Seed Grant under IoE Scheme. The financial support from CSIR [Grant no. 01 (2977)/19/EMR-II], Govt. of India is acknowledged by Dr. Arindam Indra. Baghendra Singh acknowledges DST-INSPIRE [IF180147] for providing financial support. Jitendra Kumar Yadav acknowledges CSIR, INDIA for senior research fellowship and Sarvesh Kumar Pal thanks UGC, INDIA for JRF. Prem Lama gratefully acknowledges financial support from the Department of Science and Technology (DST), New Delhi in the form of a DST-INSPIRE Faculty award [DST/INSPIRE/04/2017/000249]. Authors also acknowledge the CDC (Central Discovery Centre), BHU and (SATHI, BHU) for providing the electrochemical analysis facilities. We glad to acknowledge Ms. Anjali Mishra, BHU and Mr. Gaurav Kumar Mishra, University of Delhi, for their help in electrochemical studies in homogeneous condition.

References

1. V. S. Thoi, Y. Sun, J. R. Long and C. J. Chang, *Chem. Soc. Rev.*, 2013, **42**, 2388-2400.
2. L. Schlapbach and A. Züttel, in *Materials for sustainable energy: a collection of peer-reviewed research and review articles from nature publishing group*, World Scientific, 2011, pp. 265-270.
3. B. Singh, O. Prakash, P. Maiti, P. W. Menezes and A. Indra, *Chem. Commun.*, 2020, **56**, 15036-15039.
4. B. Singh and A. Indra, *Mater. Today Chem.*, 2020, **16**, 100239.
5. B. Singh and A. Indra, *Mater. Today Energy*, 2020, **16**, 100404.
6. M. D. Karkas, O. Verho, E. V. Johnston and B. r. Åkermark, *Chem. Rev.*, 2014, **114**, 11863-12001.
7. K. E. Dalle, J. Warnan, J. J. Leung, B. Reuillard, I. S. Karmel and E. Reisner, *Chem. Rev.*, 2019, **119**, 2752-2875.
8. J. L. Dempsey, B. S. Brunschwig, J. R. Winkler and H. B. Gray, *Acc. Chem. Res.*, 2009, **42**, 1995-2004.
9. X. Hu, B. S. Brunschwig and J. C. Peters, *J. Am. Chem. Soc.*, 2007, **129**, 8988-8998.
10. B. J. Fisher and R. Eisenberg, *J. Am. Chem. Soc.*, 1980, **102**, 7361-7363.
11. J. Hawecker, J. M. Lehn and R. Ziessel, *New J. Chem.*, 1983, **7**, 271.
12. M. Razavet, V. Artero and M. Fontecave, *Inorg. Chem.*, 2005, **44**, 4786.
13. E. S. Andreiadis, P. A. Jacques, P. D. Tran, A. Leyris, M. Chavarot-Kerlidou, B. Jousselme, M. Matheron, J. Pécaut, S. Palacin, M. Fontecave and V. Artero, *Nat. Chem.*, 2013, **5**, 48-53.
14. N. Elgrishi, S. Griveau, M. B. Chambers, F. Bedioui and M. Fontecave, *Chem. Commun.*, 2015, **51**, 2995-2998.
15. D. Aand, S. Sk, K. Kumar, U. Pal and A. K. Singh, *Int. J. Hydrog. Energy*, 2022, **47**, 7180-7188.
16. S. Roy, Z. Huang, A. Bhunia, A. Castner, A. K. Gupta, X. Zou and S. Ott, *J. Am. Chem. Soc.*, 2019, **141**, 15942-15950.
17. T. Banerjee, F. Haase, G. k. Savasci, K. Gottschling, C. Ochsenfeld and B. V. Lotsch, *J. Am. Chem. Soc.*, 2017, **139**, 16228-16234.
18. K. Kumar and B. D. Gupta, *J. Organomet. Chem.*, 2011, **696**, 3785-3791.
19. G. Dutta, K. Kumar and B. Gupta, *Organometallics*, 2009, **28**, 3485-3491.

20. B. Reuillard, J. Warnan, J. J. Leung, D. W. Wakerley and E. Reisner, *Angew. Chem.*, 2016, **128**, 4020-4025.
21. I. K. Sideri, G. Charalambidis, A. G. Coutsolelos, R. Arenal and N. Tagmatarchis, *Nanomaterials*, 2022, **12**, 3077.
22. E. Benazzi, F. Begato, A. Niorettini, L. Destro, K. Wurst, G. Licini, S. Agnoli, C. Zonta and M. Natali, *J. Mater. Chem. A*, 2021, **9**, 20032-20039.
23. D. Dolui, S. Khandelwal, P. Majumder and A. Dutta, *Chem. Commun.*, 2020, **56**, 8166-8181.
24. N. M. Muresan, J. Willkomm, D. Mersch, Y. Vaynzof and E. Reisner, *Angew. Chem.*, 2012, **124**, 12921-12925.
25. C. M. Margonis, M. Ho, B. D. Travis, W. W. Brennessel and W. R. McNamara, *Chem. Commun.*, 2021, **57**, 7697-7700.
26. A. Indra, B. Singh and A. Yadav, *J. Mater. Chem. A*, 2022.
27. B. Singh, A. Singh, A. Yadav and A. Indra, *Coord. Chem. Rev.*, 2021, **447**, 214144.
28. B. Singh and A. Indra, *Chem. Asian J.*, 2020, **15**, 607-623.
29. A. Indra, U. Paik and T. Song, *Angew. Chem. Int. Ed.*, 2018, **57**, 1241-1245.
30. B. Singh and A. Indra, *Inorg. Chim. Acta*, 2020, **506**, 119440.
31. Y. Chen, H. Chen and H. Tian, *Chem. Commun.*, 2015, **51**, 11508-11511.
32. A. Indra, P. W. Menezes, I. Zaharieva, H. Dau and M. Driess, *J. Mater. Chem. A*, 2020, **8**, 2637-2643.
33. B. Singh, A. K. Patel and A. Indra, *Mater. Today Chem.*, 2022, **25**, 100930.
34. Y. Yan, B. Y. Xia, B. Zhao and X. Wang, *J. Mater. Chem. A*, 2016, **4**, 17587-17603.
35. S. Pan, H. Li, D. Liu, R. Huang, X. Pan, D. Ren, J. Li, M. Shakouri, Q. Zhang and M. Wang, *Nat. Commun.*, 2022, **13**, 1-10.
36. D. Dolui, A. Q. Mir and A. Dutta, *Chem. Commun.*, 2020, **56**, 14841-14844.
37. N. Mahmood, Y. Yao, J. W. Zhang, L. Pan, X. Zhang and J. J. Zou, *Adv. Sci.*, 2018, **5**, 1700464.
38. A. Panagiotopoulos, K. Ladomenou, D. Sun, V. Artero and A. G. Coutsolelos, *Dalton Trans.*, 2016, **45**, 6732-6738.
39. P. Raj, A. Singh, A. Singh and N. Singh, *Dalton Trans.*, 2017, **46**, 985-994.
40. X. Yu, J. Guo, P. Peng, F. Shen, Y. Li, L. Geng and T. Wang, *Appl. Surf. Sci.*, 2019, **487**, 473-479.
41. S. Nayak, P. Das and K. Sahoo, *CHEMICAL PAPERS-SLOVAK ACADEMY OF SCIENCES*, 2003, **57**, 91-96.

42. G. Dutta and B. Gupta, *J. Organomet. Chem.*, 2011, **696**, 2693-2701.
43. C. Lopez, S. Alvarez, X. Solans and M. Font-Altaba, *Inorg. Chem.*, 1986, **25**, 2962-2969.
44. S. Mirra, M. Strianese, C. Pellecchia, V. Bertolasi, G. Monaco and S. Milione, *Inorg. Chim. Acta*, 2016, **444**, 202-208.
45. D. W. Wakerley and E. Reisner, *PCCP*, 2014, **16**, 5739-5746.
46. X. Li, H. Lei, X. Guo, X. Zhao, S. Ding, X. Gao, W. Zhang and R. Cao, *ChemSusChem*, 2017, **10**, 4632-4641.
47. T. Fang, L.-Z. Fu, L.-L. Zhou, S.-Z. Zhan and S. Chen, *Electrochim. Acta*, 2015, **178**, 368-373.
48. H. S. Ahn, T. C. Davenport and T. D. Tilley, *Chem. Commun.*, 2014, **50**, 3834-3837.
49. M. Tohidinia, A. Biabangard and M. Noroozifar, *RSC Adv.*, 2020, **10**, 2944-2951.
50. A. L. Eckermann, D. J. Feld, J. A. Shaw and T. J. Meade, *Coord. Chem. Rev.*, 2010, **254**, 1769-1802.
51. T. Shinagawa, A. T. Garcia-Esparza and K. Takanabe, *Sci. Rep.*, 2015, **5**, 1-21.
52. Y.-H. Fang and Z.-P. Liu, *ACS Catal.*, 2014, **4**, 4364-4376.
53. J. Jia, L. C. Seitz, J. D. Benck, Y. Huo, Y. Chen, J. W. D. Ng, T. Bilir, J. S. Harris and T. F. Jaramillo, *Nat. Commun.*, 2016, **7**, 1-6.
54. A. Paracchino, V. Laporte, K. Sivula, M. Grätzel and E. Thimsen, *Nat. Mater.*, 2011, **10**, 456-461.
55. I. M. Mosa, S. Biswas, A. M. El-Sawy, V. Botu, C. Guild, W. Song, R. Ramprasad, J. F. Rusling and S. L. Suib, *J. Mater. Chem. A*, 2016, **4**, 620-631.
56. V. Artero, M. Chavarot-Kerlidou and M. Fontecave, *Angew. Chem. Int. Ed.*, 2011, **50**, 7238-7266.
57. B. S. Furniss, *Vogel's textbook of practical organic chemistry*, Pearson Education India, 1989.
58. N. SAINT, *Inc.: Madison, WI*, 2003.
59. S. G. SADABS, *Bruker AXS Inc.: Madison, WI*, 2002.
60. R. H. Blessing, *Acta Crystallogr. Sect. A: Found. Crystallogr.*, 1995, **51**, 33-38.
61. G. Sheldrick, *Acta Crystallographica Section A*, 2008, **64**, 112-122.
62. L. J. Barbour, *J. Appl. Crystallogr.*, 2020, **53**, 1141-1146.
63. B. Singh and A. Indra, *Dalton Trans.*, 2021, **50**, 2359-2363.